Annals of Biomedical Engineering (© 2020)
https://doi.org/10.1007/s10439-020-02474-4

BMES BIOMEDICAL ENGINEERING SOCIETY

Biomaterials - Engineering Cell Behavior

Targeted Intravenous Nanoparticle Delivery: Role of Flow and Endothelial Glycocalyx Integrity

MING J. CHENG,[1,6,7] RONODEEP MITRA,[1] CHINEDU C. OKORAFOR,[1] ALINA A. NERSESYAN,[2] IAN C. HARDING,[2] NANDITA N. BAL,[1] RAJIV KUMAR,[3,8] HANJOONG JO,[4] SRINIVAS SRIDHAR,[3] and ENO E. EBONG[1,2,5]

[1]Department of Chemical Engineering, Northeastern University, 360 Huntington Avenue, 313 Snell Engineering Building, Boston, MA 02115, USA; [2]Department of Bioengineering, Northeastern University, Boston, MA, USA; [3]Department of Physics, Northeastern University, Boston, MA, USA; [4]Department of Biomedical Engineering, Emory University and Georgia Institute of Technology, Atlanta, GA, USA; [5]Department of Neuroscience, Albert Einstein College of Medicine, New York, NY, USA; [6]Department of Neurology, The Massachusetts General Hospital, Boston, MA, USA; [7]The NeuroDiscovery Center, Harvard Medical School, Boston, MA, USA; and [8]R&D Biomedical Materials, Millipore Sigma (A Business of Merck KGaA, Darmstadt, Germany), Milwaukee, WI, USA

(*Received 21 August 2019; accepted 4 February 2020*)

Associate Editor Debra T. Auguste oversaw the review of this article.

Abstract—Therapies for atherosclerotic cardiovascular disease should target early disease stages and specific vascular sites where disease occurs. Endothelial glycocalyx (GCX) degradation compromises endothelial barrier function and increases vascular permeability. This initiates pro-atherosclerotic lipids and inflammatory cells to penetrate vessel walls, and at the same time this can be leveraged for targeted drug delivery. In prior cell culture studies, GCX degradation significantly increased endothelial cell uptake of nanoparticle vehicles that are designed for drug delivery, compared to the effects of intact GCX. The present study assessed if the cell culture findings translate to selective nanoparticle uptake in animal vessels. In mice, the left carotid artery (LCA) was partially ligated to disturb blood flow, which induces GCX degradation, endothelial dysfunction, and atherosclerosis. After ligation, the LCA vessel wall exhibited a loss of continuity of the GCX layer on the intima. 10-nm gold nanospheres (GNS) coated with polyethylene glycol (PEG) were delivered intravenously. GCX degradation in the ligated LCA correlated to increased GNS infiltration of the ligated LCA wall. This suggests that GCX dysfunction, which coincides with atherosclerosis, can indeed be targeted for enhanced drug delivery, offering a new approach in cardiovascular disease therapy.

Keywords—Endothelial cells, Blood vessels, Atherosclerosis, Disturbed flow, Glycocalyx, Nanoparticle.

Address correspondence to Eno E. Ebong, Department of Chemical Engineering, Northeastern University, 360 Huntington Avenue, 313 Snell Engineering Building, Boston, MA 02115, USA. Electronic mail: e.ebong@northeastern.edu

ABBREVIATIONS

ANOVA	Analysis of variance
BSA	Bovine serum albumin
DAPI	4′,6-diamidino-2-phenylindole
DLS	Dynamic light scattering
ECA	External carotid artery
EGM-2	Endothelial cell growth medium-2
GCX	Glycocalyx
GNS	Gold nanospheres
HepIII	Heparinase III
HS	Heparan sulfate
HUVEC	Human umbilical vein endothelial cells
IACUC	Institutional Animal Care and Use Committee
ICA	Internal carotid artery
LCA	Left carotid artery
NHS	*N*-Hydroxysuccinimide
OA	Occipital artery
OCT	Optimal cutting temperatire
PBS	Phosphate buffered saline
PEG	Polyethylene glycol
RCA	Right carotid artery
SEM	Standard error of the mean
SH–PEG–COOH	PEG with a thiol (SH) group and a carboxyl (COOH) group
SH–PEG–NH_2	PEG with a thiol (SH) group and an amide (NH_2) group

Published online: 18 February 2020

$SH–PEG–OCH_3$	PEG with a thiol (SH) group and a methoxy (OCH_3) group
TEM	Transmission electron microscopy
THPC	Tetrakis-(hydroxymethyl)-phosphonium chloride
TSA	Tyramide signal amplification
WGA	Wheat germ agglutinin

INTRODUCTION

Cardiovascular diseases, such as those derived from atherosclerotic vessel hardening due to cholesterol- and macrophage-filled plaque formation, are the leading causes of death worldwide.[18] These diseases remain prevalent despite significant treatment advances and efforts to mitigate their progression, for a number of reasons. Statin therapy, for example, is a relatively successful treatment measure against timely diagnosed cardiovascular disease.[24] However, statins' impacts are systemic throughout the body and statin use has been associated with muscle and liver damage, type 2 diabetes, and neurological side effects.[24] Since atherosclerosis develops over a long timescale of decades, statins can be unfavorable for long-term treatment, due to the adverse effects.[24] Late detection of atherosclerosis, which can coincide with a heart related incident or other severe cardiovascular events, requires treatment that is more invasive than statin administration. Surgical angioplasty, stent placement, or bypass of a damaged artery *via* a replacement vessel are examples of highly invasive treatments.[8] These procedures can fail due to mechanical damage to the blood vessel wall, biomaterial incompatibility, or mismatch between the replacement vessel and the host vessel, despite occasional co-delivery with therapeutics intended to combat complications after surgery.[3,9,12] New approaches should be developed to treat atherosclerosis at early disease stages, at specific affected vascular sites, and preferably in a manner that is non-invasive.

Towards this end, we turn our attention to the nanoscale endothelium surface glycocalyx (GCX), which is an extracellular matrix bound to and encapsulating the endothelial cells lining the blood vessel wall. This GCX is of great interest, with respect to improving atherosclerosis treatment, because initiation and development of atherosclerotic plaques have been correlated to its dysfunction.[17] In healthy conditions, the GCX plays a key role in maintaining endothelial cell functions that lead to vessel health, while providing a vascular permeability barrier.[14,25] These functions are derived from the GCX structure, which has compositional diversity across vessel types and species.[11] Generally, the GCX is composed of tethered glycosaminoglycans, anchoring proteoglycans, bound glycoproteins, and adsorbed soluble molecules which endow the GCX with a nanoscale brush-like structure, a net negative charge, an average pore size of 7 nm, and an overall thickness reported in the range of nanometers to several microns.[11,32] It is important to note here that the most extensively studied GCX components, and the primary focus of the study described herein, are the glycosaminoglycans, such as those identified as heparan sulfate (HS), hyaluronic acid, and chondroitin sulfate, along with sialic acid modified glycoproteins. The glycosaminoglycans are constantly degraded through enzymes, and in turn they are synthesized and extruded *via* vesicles of the Golgi apparatus, to maintain homeostatic balance.[29] This homeostasis breaks down and GCX shedding occurs in disease conditions such as hypertension, diabetes, kidney disease, and albuminuria, which are associated with increased risk of atherosclerosis.[16,34,37] Patients are also prone to GCX damage from angioplasty and bypass surgeries.[31] Low magnitude and inconsistent blood flow conditions can also cause damage to the GCX.[20] Loss of the vasculoprotective GCX due to any one of these reasons can result in compromised endothelial barrier function, characterized by an increase in vessel permeability. Downstream, this leads to unwanted cholesterol and macrophage infiltration of the vessel wall, causing atherosclerosis.

GCX degradation should not only be accepted as occurring in association with atherosclerosis, but it should also be leveraged to improve the approach to atherosclerosis treatment. It should be leveraged to replace systemic anti-atherosclerosis drug delivery approaches with localized drug delivery. Furthermore, if a nanoscale drug carrier is used, leveraging a permeable GCX can be done in a minimally invasive manner. Therefore, we hypothesize that nanoparticle-based drug delivery strategies are well suited to take advantage of dysfunctional GCX for early, targeted, and minimally invasive anti-atherosclerotic treatment.

In support of our hypothesis, we performed previous studies demonstrating elevated uptake of ultrasmall nanoparticles by cultured endothelium exhibiting GCX degradation due to heparinase III (HepIII) enzyme in the environment or due to disruptions in the flow that has direct impact on the endothelial surface.[5,6] Ultrasmall nanoparticles were chosen over typically sized (50–200 nm) nanoparticles, in consideration of the 7-nm pore size of the GCX, to maximize delivery of the nanoparticles to sites affected by even minor structural degradation of the GCX. These particles also possessed a net negative charge, which facilitates their repulsion by an intact negatively charged GCX and, on the other hand, allows their

passive penetration through a degraded GCX. It is questionable, however, whether these findings will apply beyond the cell culture experiments and extend to animal models and humans. The native *in vivo* environment incorporates undulating movements of the vessel walls, pulsatile flow, and various circulating blood cells and molecules that can have an effect on the GCX and endothelial cells. Furthermore, immune and renal systems hinder nanoparticle activity by opening up avenues for the particles to be removed from regions of interest.[39]

Therefore, an animal study was performed to further test our hypothesis in the complex *in vivo* environment. We focused on the early stages of disease by working with chow fed C57BL/6 mice that are slow to develop atherosclerosis,[27] as opposed to working with conventionally used high fat diet fed apolipoprotein-E-deficient mice that are programmed to develop accelerated atherosclerosis.[27] We attempted to induce onset of GCX degradation in the mice by performing a surgical partial ligation of the left carotid artery (LCA). The non-ligated right carotid artery (RCA) in each mouse was a healthy and intact counterpart to the LCA, enabling comparison to a reference condition. Compared to the RCA, the LCA ligation was not only invasive but it also dramatically disturbed the flow of blood, caused endothelial dysfunction and subsequent GCX degradation, and induced vessel remodeling, as previously shown.[15,21,23] After the mice were intravenously treated with ultrasmall nanoparticles, we examined the mice and found that the ultrasmall nanoparticles circulating in blood eventually were localized selectively in the walls of the dysfunctional and GCX-deficient LCA, as compared to the walls of the RCA. Our finding provides additional evidence that degraded GCX can be leveraged for delivery of nanoparticles at time points associated with atherosclerosis initiation and to targeted vascular locations. We anticipate that, in the future, these nanoparticles, once they are further functionalized, can be used to improve the delivery and the efficacy of anti-atherosclerosis drugs.

MATERIALS AND METHODS

Nanoparticle Fabrication and Characterization for In Vivo and In Vitro Experiments

Ultra-small gold nanospheres (GNS) coated with polyethelyne glycol (PEG) were fabricated as described in previous publications.[5–7] In brief, tetrakis-(hydroxymethyl)-phosphonium chloride (THPC)-coated GNS were first formed (Fig. 1a). Subsequently, PEGylation of the THPC-coated GNS was done by a ligand exchange process using heterobifunctional PEGs: methoxy(OCH_3)-PEG-thiol(SH), carboxyl(COOH)-PEG-SH, and amide(NH_2)-PEG-SH (Fig. 1a). The PEG provides biocompatibility and extends blood circulation time and the COOH or NH_2 groups can be conjugated with therapeutic, targeting, and visualization ligands.[4] For imaging of the GNS in this study, the SH–PEG–NH_2 was conjugated with a fluorophore in the form of N-Hydroxysuccinimide (NHS) ester groups of biotin, for *in vivo* imaging, or Alexa Flour 647, for *in vitro* imaging (Fig. 1a). Fabricating consistently ultra-small PEG-coated GNS was of great importance in this project and confirmed using a (Fig. 1b) transmission electron microscope (TEM) (JEOL JEM-1000, Tokyo, Japan), at 80 kV and ×150,000 magnification, and by performing (Fig. 1c) dynamic light scattering (DLS) (Brookhaven 90Plus Particle Size Analyzer; Brookhaven Instruments Corporation, Holtsville, NY, USA). Other details of the GNS characterization are described in our prior publications.[5–7]

Animal Experiments

Animal studies were approved by the Northeastern University Institutional Animal Care and Use Committee (NU-IACUC) and Emory University Institutional Animal Care and Use Committee (IACUC). Animals were purchased from Jackson Laboratories, fed a chow diet and water, and were allowed to acclimate for 1 week before experimentation.

Partial Carotid Surgery

Seven C57BL/6 male mice at 4 weeks of age underwent the partial LCA ligation surgery, for induction of acute disturbed flow, which has been reported to induce GCX degradation and endothelial dysfunction.[15,21,23] Surgeries were performed, as described in the *Supplementary Materials and Methods* document, to ligate the external carotid artery (ECA) branch on its own and to ligate the internal carotid artery (ICA) and occipital artery (OA) branches together (Fig. 2). The superior thyroid artery (STA) was left untouched (Fig. 2). Ultrasound was used to confirm the effect of ligation on blood flow in the LCA compared to the RCA (reference vessel). During the period of acclimation after the LCA ligation surgery, mice were housed in the IACUC animal facilities for 4 weeks with daily checks to ensure recovery without complications (Fig. 2).

Nanoparticle Administration In Vivo

At day 26 after LCA ligation, anesthetized mice intravenously received 25 mg of biotin-conjugated PEGylated GNS in 150 μL of sterile phosphate buf-

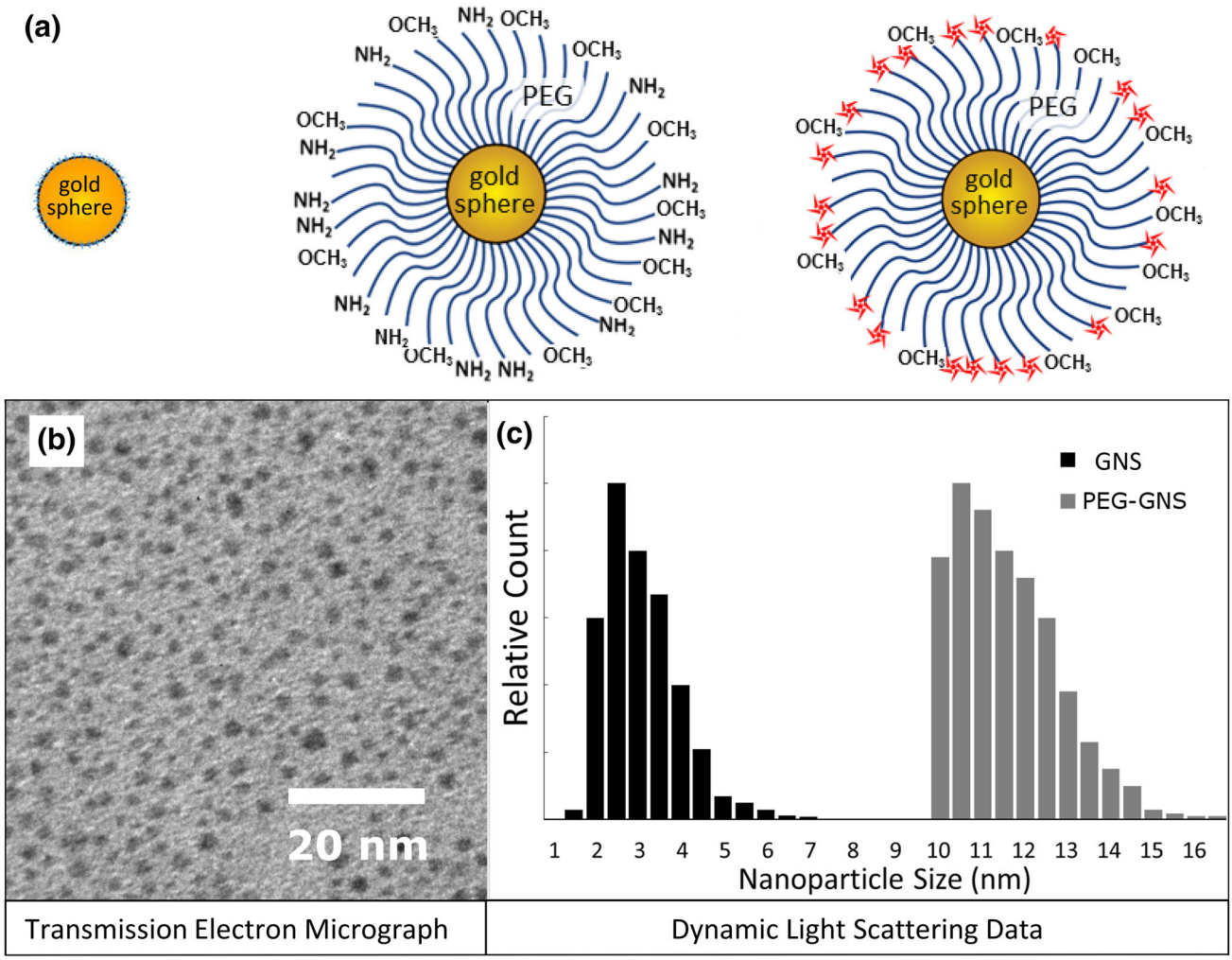

FIGURE 1. (a) Schematic of gold nanoparticle coated with polyethylene glycol (PEG). The OCH_3, COOH, and NH_2 functional groups on PEG allow for conjugation and customization of nanoparticles, for specific targeting, drug delivery, and imaging. In this project, biotin is conjugated to NH_2 for *in vivo* imaging or fluorescence is conjugated to NH_2 for *in vitro* imaging. (b) TEM shows that the gold core has a diameter of 2–4 nm. (c) Dynamic light scattering (DLS) confirms the TEM results for the bare gold core and also shows that the PEG coating increases the nanoparticle diameter to 10–12 nm. Figures and data re-used with permission from Cheng *et al.* J Vis Exp.[7].

fered saline (PBS) (Fig. 2). Mice were allowed to rest for 48 h (Fig. 2). See *Supplementary Materials and Methods* for more details.

Euthanasia, Fixation, and Carotid Artery Isolation

As described in the *Supplementary Materials and Methods* document, the animals were euthanized, fixed, and dissected 28 days post-ligation surgery, 2 days after GNS treatment (Fig. 2). The carotids along with the aortic arch were extracted and stored in PBS.

Cryopreservation, Cryostat Sectioning, and Staining

The LCA and RCA were separately embedded in optimal cutting temperature (OCT) compound and cryopreserved at liquid nitrogen temperature (Fig. 2). Both arteries were then cryosectioned into 6 μm slices (Fig. 2).

Flourescent staining of GNS uptake into the vessel wall and GCX expression on the vessel wall were performed as described in the *Supplementary Materials and Methods* document. Briefly, the LCA and RCA slices were post-fixed and permeabilized, antigens were retrieved, and non-specific binding sites were blocked. The biotin-coated PEGylated GNS within the LCA and RCA slices were labeled (Fig. 2) with streptavidin conjugated with horseradish peroxidase. To label the GCX (Fig. 2), the LCA and RCA slices were incubated with wheat germ agglutinin (WGA), which is a lectin that labels a number of GCX components, including sialic acid and *N*-acetylglucosamine which is a com-

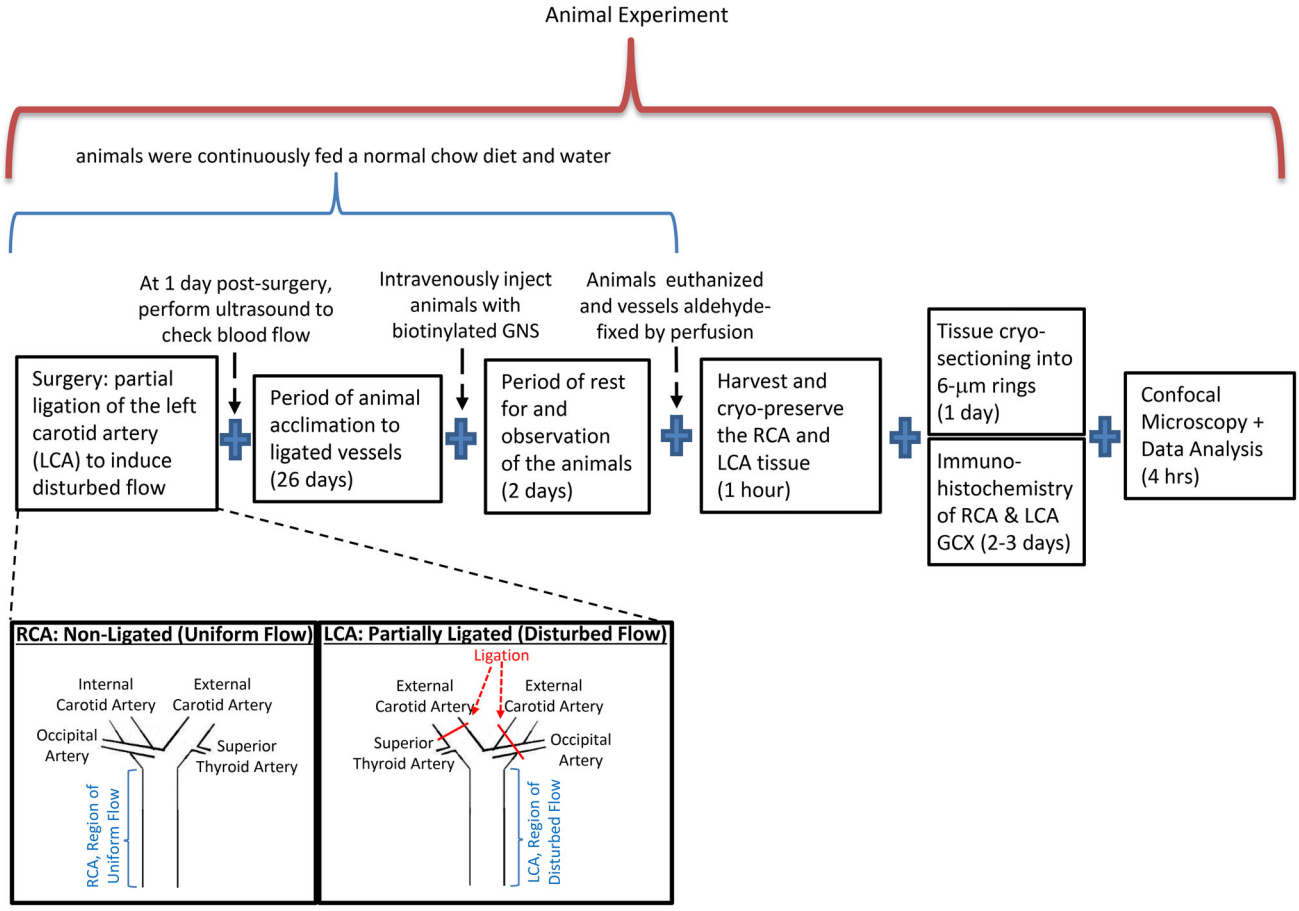

FIGURE 2. Animal experiment procedure.

ponent of HS and hyaluronic acid.[33] WGA was followed by streptavidin conjugated with horseradish peroxidase. After the GNS or GCX were labeled with horseradish peroxidase-conjugated streptavidin, a tyramide signal amplification (TSA) Plus Cyanine 3 amplification kit was used to add fluorescence, with amplified signal. The LCA and RCA sections were covered with Vectashield antifade mounting medium containing 4′,6-diamidino-2-phenylindole (DAPI), to mark cell nuclei. Imaging was performed using a Zeiss laser scanning confocal fluorescence microscope, to visualize DAPI labeled cell nuclei of all vessel wall cells, elastin auto-fluorescence, GNS, and WGA-labeled GCX.

Endothelial Cell Experiments

Cell Culture

Cultured human umbilical vein endothelial cells (HUVECs), purchased from ATCC (Manassas, VA), were used at passages 2 to 8 (Fig. 3) as described in the *Supplementary Materials and Methods* document. Experiments were not performed unless HUVEC were in fully confluent monolayers.

Flow and GCX Conditions

Once confluent, HUVECs were exposed for 16 h to flow conditions at a constant shear stress of 12 dynes/cm^2 (Fig. 3). To study the effect of degraded GCX, the flow was sometimes supplemented with 1.25×10^{-6} IU/mL HepIII, which specifically degrades the HS component of the GCX (Fig. 3), and at other times flow was absent (static conditions, 0 dynes/cm^2), to render GCX deficiency due to disruption of flow. HUVECs stimulated by flow with or without HepIII, or exposed to static conditions, were fixed and stained for HS using 1:100 10E4 epitope anti-HS and 1:1000 Alexa Fluor 488 conjugated goat anti-mouse IgM (Fig. 3). DAPI was used to label cell nuclei. See *Supplementary Materials and Methods* for more details. Imaging was previously described.[5]

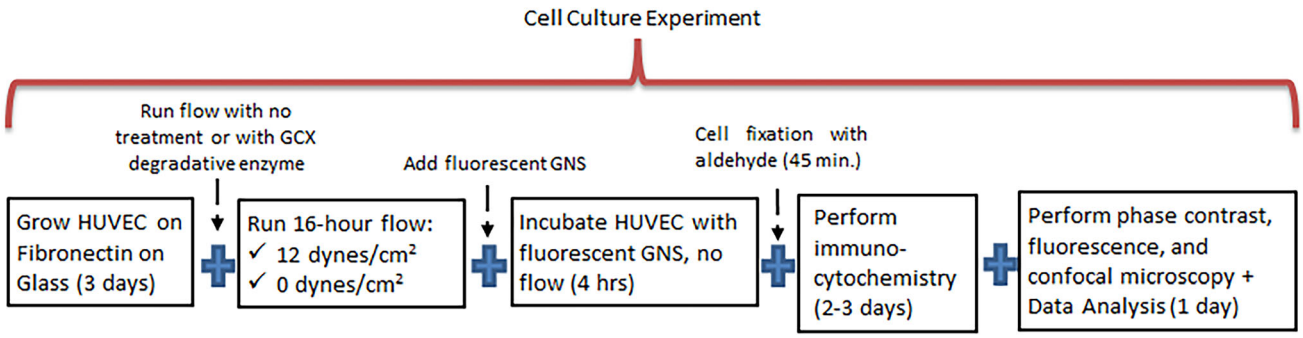

FIGURE 3. Cell culture experiment procedure.

HUVEC Interaction with GNS

After the 16-h period of 0 or 12 dynes/cm^2 flow-conditions, in the presence or absence of HepIII, the HUVECs were cultured with 500 μg/mL of Alexa Flour 647 conjugated PEGylated GNS, for 4 h (Fig. 3). See *Supplementary Materials and Methods* for more details.

Imaging and Data Acquisition

Fluorescently labeled sections of LCA, sections of RCA, and monolayers of HUVEC were imaged under confocal microscopy as described previously and in *Supplementary Materials and Methods* (Figs. 2 and 3).[5,6,21] Analysis was performed using NIH ImageJ software. For detailed methods, please refer to the *Supplementary Materials and Methods* document.

Statistics

Data were expressed as mean ± SEM. Graph Pad Prism software was used to perform analysis of variance (ANOVA) statistical analysis, followed by *post hoc* analysis *via* Tukey's Test, to determine the statistical significance of differences between means. Additional details of the statistical tests are described in figure captions.

RESULTS

Functionalized GNS Are Ultra-Small and Expected to Be Compatible with and Passively Target Degraded GCX

We first confirmed the size of the synthesized GNS, by TEM imaging at 80 kV and ×150,000 magnification. As indicated by the scale bar on the TEM images, the diameters of pre-PEGylated GNS particles ranged from 2 to 3 nm (Fig. 1b). TEM also confirmed that the THPC-coated GNS were individually dispersed. After PEGylation, increase in GNS size was not visible under TEM due to the lack of electron density of the PEG polymers, but *via* TEM it was confirmed that the GNS remained individually dispersed (data not shown). This was expected because the PEG coat on the GNS should prevent aggregation into larger sized particles. DLS was performed to measure the size of PEGylated GNS. The DLS size measurement histograms, as represented by the ones shown in Fig. 1c, revealed a GNS size peak at 2.5 nm prior to PEGylation and a shift to approximately 10.5 nm once the GNS were PEGylated.

In our previous publication, we also looked at surface charge of the PEGylated GNS. Zeta potential calculations revealed a particle charge of − 14 mV[5].

Partial Carotid Ligation Successfully Induces Disturbed Flow, Vessel Remodeling, and GCX Degradation, Mimicking Disease Conditions

In 4-week-old C57BL/6 mice we were able to successfully locate the branches of the LCA (Figs. 2 and 4a) in order to perform the partial LCA ligation surgery. Once the branches were located, the STA was left as is, and the ECA was ligated on its own while the ICA and OA were ligated together (Figs. 2 and 4a). The ligation sites are indicated by the red lines in the diagrams shown in Figs. 2 and 4a.

Using ultrasound, successful LCA ligation was confirmed to permit continued blood flow without bleeding or blockage (Fig. 4b). According to the ultrasound recording, blood flow in the contralateral non-ligated RCA, a control inherent to each mouse, remained stably unidirectional and pulsatile with a frequency of 6.7 Hz and a maximum velocity of about 325 mm/s (Fig. 4b). Compared to the RCA, LCA blood flow was bidirectional and reduced in magnitude to a velocity ranging from − 50 to 138 mm/s, at the same 6.7 Hz frequency (Fig. 4b). In a previous study, we performed computational fluid dynamics, determining that on the first day after ligation the RCA

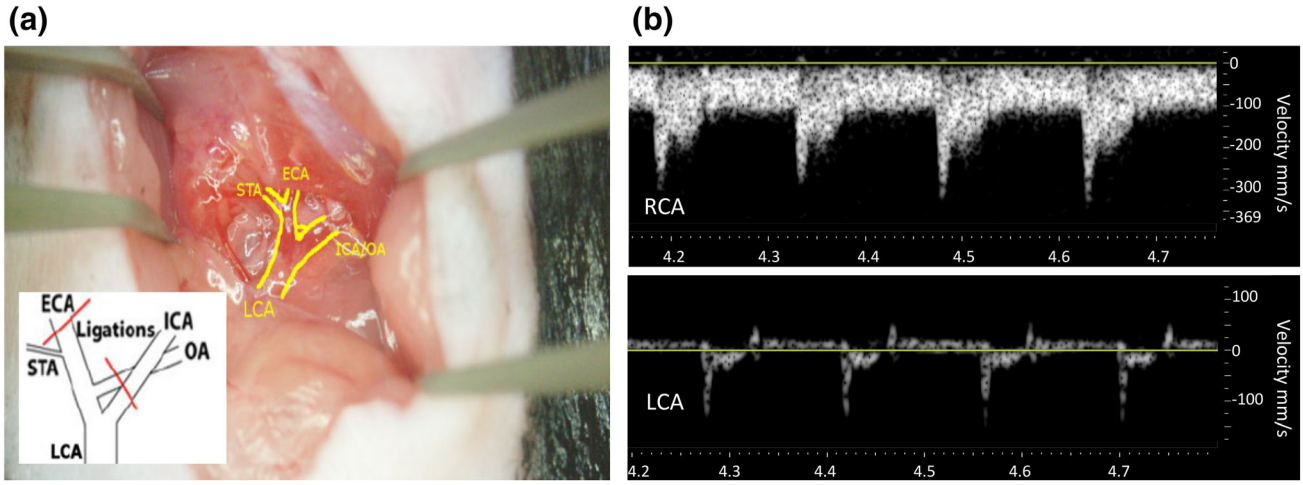

FIGURE 4. (a) Picture shows LCA and its branches (outlined in yellow) prior to surgically ligating the ECA, ICA, and OA while leaving the STA open. Schematic on the bottom left clarifies the vessels that were ligated during the surgical procedure.[23] (b) Ultrasound of mouse RCA (top) and LCA (bottom) 1 day post-ligation shows blood flow pulsatility, blood flow velocity amplitudes, and the direction of blood flow in each of the two vessels.

experiences shear stress at a range of 80–120 dynes/cm^2 while the LCA experiences shear stress of approximately 30 dynes/cm^2.[23] We anticipate that by 4 weeks after ligation the shear stress levels in the LCA and RCA will further deviate from each other, with RCA conditions remaining stable while LCA average shear stress drops. Therefore, the partial ligation model achieves the goal of creating an LCA vessel experiencing disturbed flow and the healthy RCA provides a convenient comparison to a vessel experiencing stably streamlined flow.

After the 4-week period of exposure to disturbed blood flow, compared to the RCA the difference in the LCA vessel wall was apparent to the naked eye (Fig. 5a). Upon closer inspection using immunohistology, the 4-week partial ligation of the LCA was observed to have induced significant morphological changes (Fig. 5b). Specifically, the LCA vessel wall experienced thickening compared to the RCA (Fig. 5b), similar to what was shown in a prior publication by Kumar *et al.*[15] We found that the average thickness of the RCA wall was 34.4 ± 6.8 μm (Fig. 5c). The LCA was statistically significantly 18 μm thicker, at 52.6 ± 5.5 μm (Fig. 5c). Histology of a LCA of a mouse who did not undergo the partial ligation procedure measured approximately 35 μm (data not shown), suggesting that the thickening of the LCA was due to the disturbed flow from the partial ligation surgery. These results, along with the results previously reported by Kumar *et al.*,[15] demonstrate that 4 weeks of flow disturbance in the blood stream of C57BL/6 mice can substantially remodel blood vessels.

In addition to the vessel wall thickening, the LCA also exhibited a more discontinuous GCX layer on the intima as compared to the RCA (Fig. 6). The difference in the WGA-labeled GCX is clearly visible in Fig. 6a, where the healthy RCA expresses a continuous WGA fluorescence pattern compared to the disrupted WGA fluorescence on the LCA. The WGA-labeled GCX coverage of the blood vessel wall decreased from 76.3 ± 10.2% in the RCA to 21.2 ± 5.9% in the LCA as shown in Fig. 6b. This is a statistically significant 55% decrease in coverage of the inner LCA wall. The degradation of the GCX, as indicated by the drop in WGA signal, coincides with the vessel wall thickening induced by the disturbed flow conditions.

Nanoparticles Infiltrate the Compromised LCA More Than the Healthy RCA

We assessed whether it would be possible for drug carrier vehicles, such as GNS, to selectively infiltration blood vessel walls at early disease stages and at specific vascular sites where disease occurs, by leveraging degraded GCX. Representative images of biotinylated GNS uptake in the mouse carotid arteries after partial ligation surgeries are shown in Fig. 7a. Upon quantifying the fluorescence intensity of the GNS in the images, we found that the LCA contained 744.0 ± 163.4 pixels compared with 294.0 ± 109.0 pixels for the RCA (Fig. 7b). These data translate to approximately 2.5-fold more GNS infiltration of the LCA, compared to the RCA.

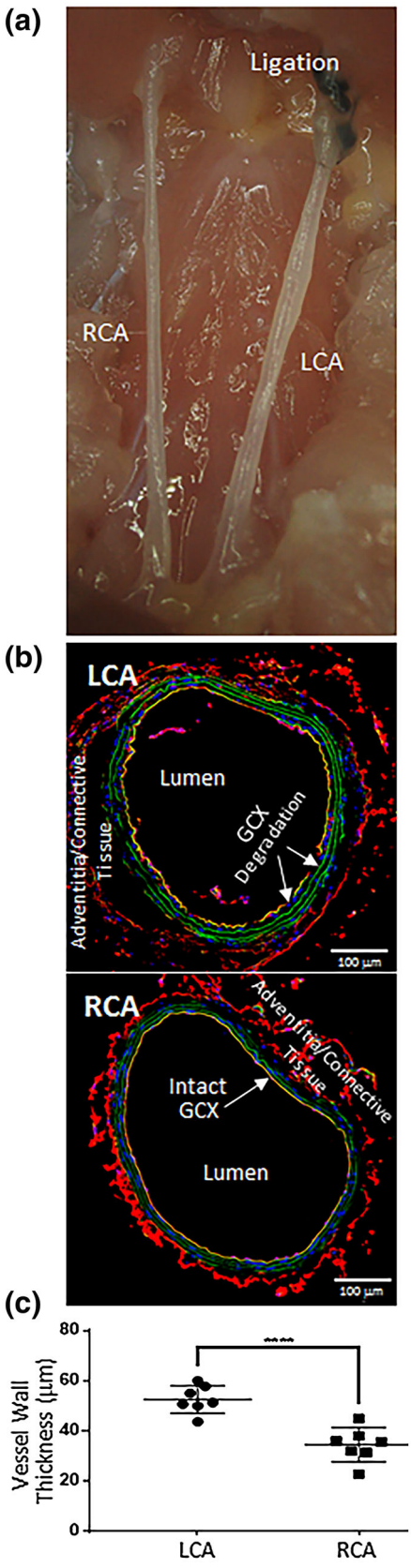

◀FIGURE 5. (a) Exposed mouse LCA and RCA, 4 weeks after partial ligation of the LCA. The black sutures from the ligation can be seen on the LCA on the top right. (b) Fluorescent images taken at ×10 magnification show histology of LCA and RCA. Cell nuclei are shown in blue. The GCX is the component shown in red and adjacent to the lumen. Adventitia/connective tissue, on the outside of the vessel, also appears in red. Green signifies elastin auto-fluorescence. GCX measurements are challenged by the low resolution of the images at ×10 magnification, but it is clear from these images that the LCA has a thicker vessel wall as compared to the RCA. (c) Plot shows the LCA and RCA wall thicknesses. The data points that are shown represent average measurements of LCA and RCA thickness for 7 mice ($N = 7$). Each average measurement was derived from nine sections per LCA and RCA, with three measurements taken from each section, for a total of twenty-seven raw data points. Statistical significance between groups is denoted as ***$P < 0.001$ (data from the RCA and LCA from the same animal were paired).

GCX Degradation: Confirmed to Promote Trans-Endothelial GNS Infiltration

Cultured HUVEC did not show any adverse morphology after 16 h of exposure to flow, static conditions, or flow in the presence of the GCX degradative enzyme, HepIII (Figs. 8a–8c). In Figs. 8d–8f fluorescent images of healthy and dysfunctional GCX are depicted. The HS stain shows a healthy HUVEC GCX under flow conditions in the absence of HepIII and lack of GCX development in HUVEC cultures exposed to static conditions or flow with HepIII. Specifically, when the GCX was visualized by labeling it with fluorescently-tagged 10E4 epitope anti-HS, the GCX on untreated and flow-conditioned HUVEC was found to be abundant (Fig. 8d), with a thickness of 1.3 ± 0.2 μm (Fig. 8j). The HS-labeled GCX covered 75 ± 4.3% of the HUVEC surface (Fig. 8h). The GCX on static-conditioned HUVEC was found to be degraded to a thickness of 0.8 ± 0.3 μm (Fig. 8e and 8j), and the extent of HUVEC coverage was degraded by 31.2 ± 14.8% (Fig. 8k). The GCX on HepIII-treated and flow-conditioned HUVEC was found to be degraded (Fig. 8f), as expected, with a thickness of 0.6 ± 0.3 μm (Fig. 8j). GCX coverage of these HUVEC was reduced by 75 ± 9.8% (Fig. 8k). These findings of significantly dissimilar GCX composition on untreated flow-conditioned HUVEC vs. static-conditioned or flow/HepIII-treated HUVEC suggest that there will be differential outcomes when it comes to endothelial uptake of GNS. As expected, the incubation of GNS with HUVEC possessing healthy vs. compromised GCX yielded a significant difference in uptake (Figs. 8g–8i). Under flow conditions in the absence of HepIII, where GCX was healthy, HUVEC were infiltrated by GNS at a normalized value of 1.00 ± 0.27 (Fig. 8i). Static conditions, which compromised the HS component of the GCX, led to HUVEC infiltration by

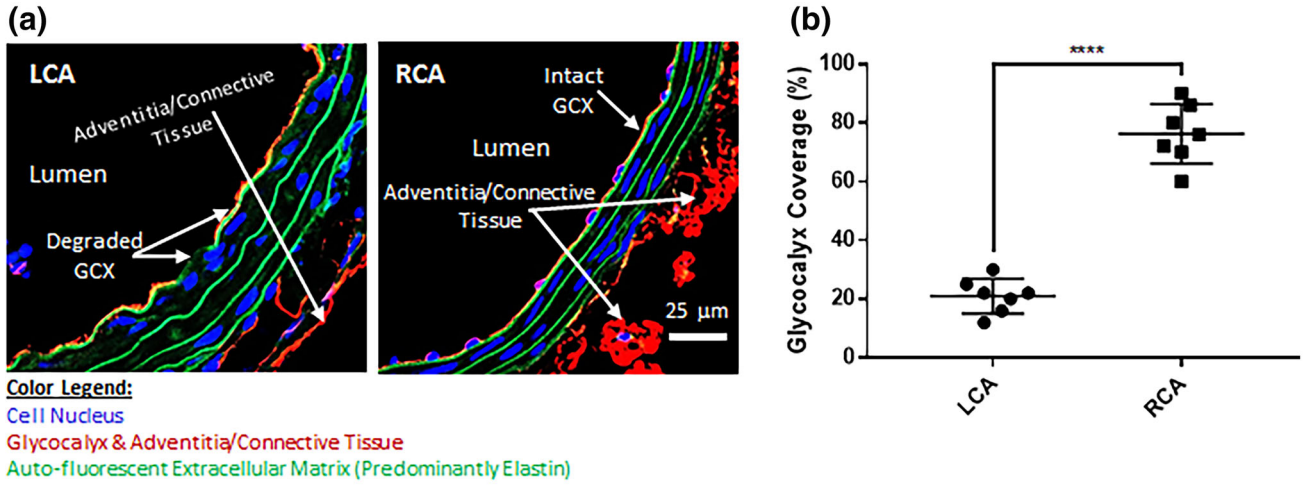

FIGURE 6. (a) Histology of mouse LCA (left) and RCA (right) at ×63 magnification. Cell nuclei are shown in blue, GCX is shown in red, and elastin is shown in green. Scale bar 25 μm. (b) Plot shows the LCA and RCA inner wall coverage by the GCX. The data points shown represent average measurements of LCA and RCA GCX coverage, for 7 mice (*N* = 7). Each average measurement comes from nine sections per LCA and RCA, with three fields of view examined per section, and three measurements taken from each field of view, for a total of 81 raw data points. Statistical significance between groups is denoted as ***$P < 0.001$ (data from the RCA and LCA from the same animal were paired).

GNS to a normalized value of 0.80 ± 0.03 (Fig. 8l). Addition of HepIII to flow conditions, which also compromised the GCX, led to a statistically significant increase in HUVEC infiltration by GNS to a normalized value of 1.94 ± 0.20 (Fig. 8i), which represents a nearly 2-fold increase compared to flow conditions in the absence of HepIII. This fold-change in infiltration due to GCX degradation in HUVEC nearly aligns with the fold-change in infiltration that we observed in our animal experiment comparing the ligated LCA to the non-ligated RCA, demonstrating the significant role that GCX degradation plays in selective GNS infiltration of dysfunctional endothelium and diseased blood vessel walls.

DISCUSSION

Initiation and localization of atherosclerosis, which is characterized by lipid and inflammatory cell penetration of vessel walls, have been strongly linked to geometrically irregular arterial regions exposed to disturbed blood flow as opposed to straight arterial regions exposed to high and stable blood flow.[35] Atherosclerosis initiation and localization have also been correlated to endothelial GCX degradation that compromises endothelial barrier function and increases vascular permeability.[14,17,25] Since our long term aim is to therapeutically address atherosclerosis at specific vascular sites where disease occurs and at early disease stages, we employed a partial vessel ligation to convert the stable shear stress conditioned LCA to a disturbed flow conditioned LCA. We examined the LCA at early onset of disturbed flow, and, furthermore, we examined the LCA in an extended disease initiation phase by using wildtype C57BL/6 mice that are typically slow to develop noticeable atherosclerosis.[27] With our approach, we were able to successfully induce disturbed flow, vessel remodeling, and GCX degradation to mimic the onset of disease conditions *in vivo*.

The extent of GCX degradation that we observed in the disturbed flow environment was substantial and informative. However, there are many components of the GCX other than the WGA-labeled components of the GCX that could have been examined in our study. The WGA-labeled GCX components include only sialic acid and the *N*-acetylglucosamine portions of HS and hyaluronic acid glycosaminoglycans.[33] We chose to use WGA because the labeled sialic acid and the *N*-acetylglucosamine GCX components are extensively expressed. In addition, sialic acid was recently shown to play a role in blood vessel wall endothelium adhesiveness,[19] which would be important for arresting the circulating GNS. The *N*-acetylglucosamine-associated HS was previously shown to be a major factor in the regulation of endothelial permeability to nanoparticles.[5,6] The *N*-acetylglucosamine-associated hyaluronic acid was also previously shown to affect vascular integrity and permeability.[30] Our study did not probe other portions of the HS and hyaluronic acid glycosaminoglycans, another glycosaminoglycan known as chondroitin sulfate, or the anchoring proteoglycans that are all additional constituents of the endothelial GCX. Monitoring the expression of these additional constituents over the course of the 4 weeks post-liga-

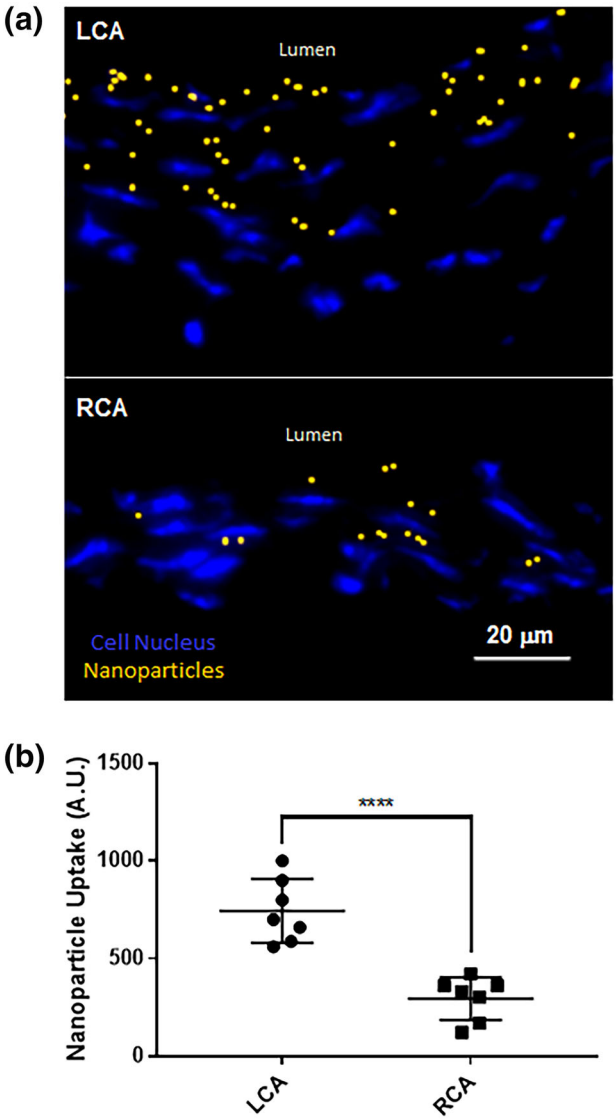

FIGURE 7. (a) Histology of mouse LCA (top) and RCA (bottom) at ×63 magnification. Cell nuclei are shown in blue and biotinylated gold nanospheres are shown in orange. (b) Quantification of LCA and RCA infiltration of fluorescent GNS is indicated by fluorescence intensity noted in terms of arbitrary units (A.U.), which represents pixels per field of view. The data points shown represent average measurements of GNS infiltration of LCA and RCA, for 7 mice (*N* = 7). Each average measurement comes from nine sections per LCA and RCA, with three fields of view examined per section, for a total of twenty-seven raw data points. Statistical significance between groups is denoted as ***$P < 0.001$ (data from the RCA and LCA from the same animal were paired). *N* = 7.

tion may have given more insight on what and how the GCX components respond to blood flow conditions and are involved in the subsequent remodeling of the carotid arteries. If it were technically feasible, it would also have been useful to perform live imaging of the GCX, which would clarify the timeline of its pathological transformation. At present, live imaging of GCX is not possible due to lack of biomarker agents that would provide sufficient resolution of the carotid artery GCX.[11] With the rapid development of imaging technology, effective and accessible live, imaging may become a reality soon. The information gained from probing multiple GCX components in live animals would inform us of the point at which GCX degradation first occurs, so that atherosclerosis therapies can be designed to truly target early disease stages.

At 10.5 nm in size and with − 14 mV surface charge, the PEGylated GNS that we synthesized were expected to be able to passively interact with the nanoscale GCX structure as it began to degrade in disturbed flow conditions. The porous structure of an intact GCX limits infiltration to water, plasma proteins such as 7-nm sized albumin, and smaller solutes,[28] while the negatively charged nature of the GCX repels negatively charged substances. Therefore, our GNS infiltration results make sense. In healthy GCX conditions, passive infiltration of the 10.5-nm, − 14 mV GNS should be limited. At vessel areas affected by GCX degradation, and even those areas of early onset of GCX degradation, passive infiltration of the GNS should be substantially higher than at vessel areas with intact GCX.

We observed GNS infiltration occurring beyond the intimal endothelial layer and reaching the medial layer, and doing so to the greatest extent in the LCA than in the RCA. We speculate that LCA wall structure and flow conditions, in addition to its degraded GCX, are key factors that influence GNS penetration of the vessel wall. The GNS initially circulate *via* the bulk flow in the blood vessel lumen, and the LCA bulk flow pattern is slow and oscillatory. Therefore, GNS in the LCA will have higher residence time for interaction with the blood vessel wall before penetration into the intimal and medial layer. A close look at the disturbed flow conditioned LCA, compared to the RCA, also reveals a structural change that the nanoparticles can leverage for medial penetration. This change includes thickening of the wall (in correlation to GCX degradation) without increases in cell density or without apparent increases in connective tissue (i.e., elastin) density. This suggests that void spaces have been created in the LCA structure. These newly created LCA void spaces will provide physical room for elevated nanoparticle penetration in the LCA, compared to the RCA. These LCA spaces will also allow room for increased interstitial flow,[35] which will push nanoparticles to more deeply penetrate the blood vessel wall.

Clearly, the GNS studied herein have room for refinement, thanks to the multiple functional groups on their surfaces. Considering that atherosclerosis initiation is correlated with GCX damage and endothelial dysfunction, in future studies the GNS

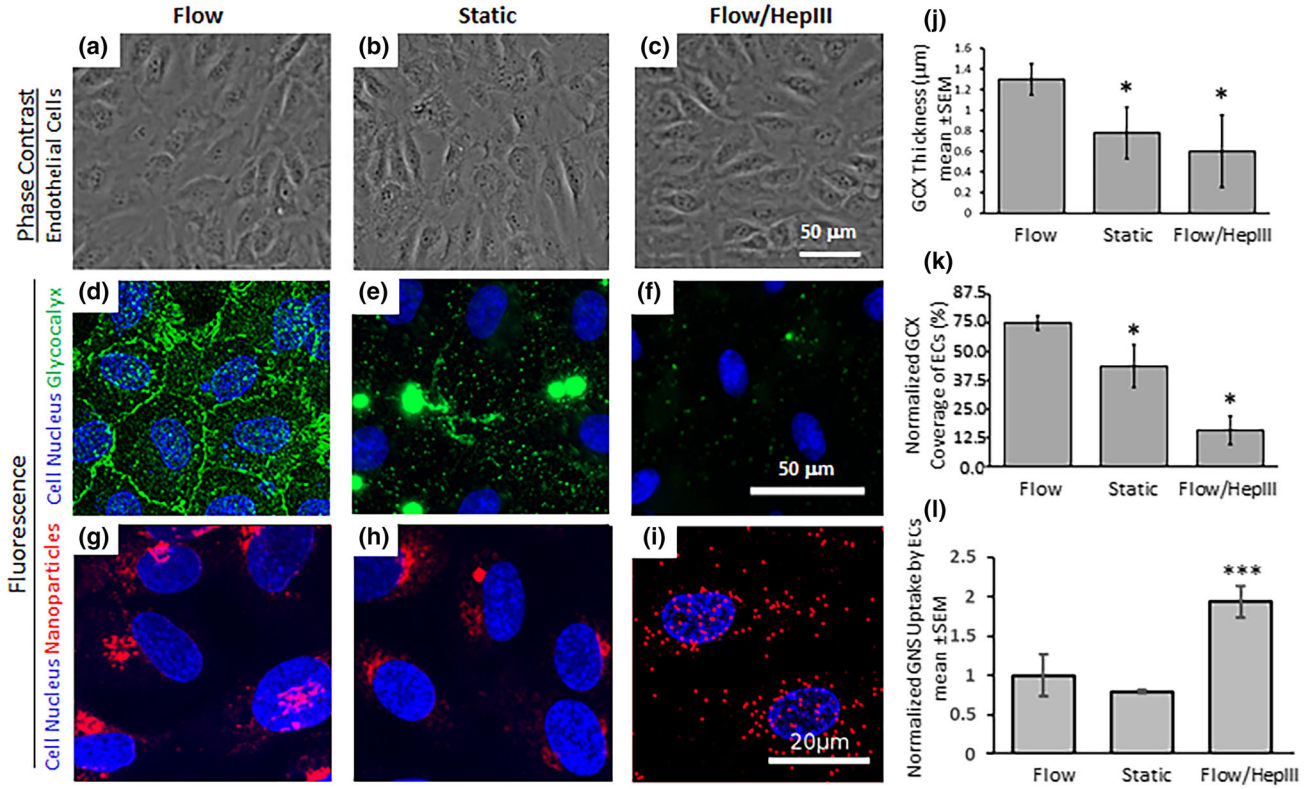

FIGURE 8. (a–c) Phase contrast images indicate HUVEC health in culture after 16 h of static (0 dynes/cm^2) conditions (b) or 16 h of 12 dynes/cm^2 shear stress flow in the absence (a) or presence (c) of HepIII enzyme which degrades the HS component of the GCX. (d–f) Confocal images of cultured HUVEC stained in green for the HS component of GCX, with the cell nuclei stained in blue. (g–i) Uptake of red fluorescent nanoparticles after 4 h of co-incubation with HUVEC at 500 μg/mL, immediately following cell exposure to flow in the absence of HepIII GCX degradative enzyme (g), static conditions (h), or flow in the presence of HepIII GCX degradative enzyme (i); cell nuclei are stained blue. (j) Quantification of "GCX Thickness" ($N = 3$) on HUVEC. (k) Quantification of "GCX Coverage" ($N = 3$) on HUVEC. (l) Quantification of "GNS Uptake" ($N = 5$) by HUVEC, with the data normalized relative to the results from baseline conditions (flow condition in the absence of GCX degradative enzyme). (a–f, j–k) Some pictures and plots are re-used with formal written permission from the publisher.[5] (j–l) All results are presented as mean ± SEM, and statistical significance compared to baseline conditions is denoted as $^*P < 0.05$ or $^{***}P < 0.001$.

should not simply be allowed to passively infiltrate the remodeled GCX and medial compartment of the blood vessel walls. Instead, the GNS should be made to actively target GCX-deficient endothelial cells, by conjugating one of the GNS functional groups to a ligand that is specific to dysfunctional endothelial cells. An active moiety specifically targeting adhesion molecules expressed on the surface of dysfunctional endothelial cells and uncovered when the GCX is shed[2] could improve localization in regions of interest and at early disease stages. Another functional group on the GNS can be conjugated with a therapeutic agent. In the future, such iterations of our GNS will enable endothelial-targeted drug delivery at early stages of vascular dysfunction. The caveat is that the small size of the GNS offers limited surface area for conjugation of active targeting ligands and drugs to be delivered.[7] Furthermore, attaching ligands or drugs onto the PEGylated GNS for active targeting and therapeutic purposes, respectively, will impact the size of the nanoparticle and slow the rate of infiltration into diseased vessel walls.[7] Therefore, future iterations of this PEGylated GNS would have to be developed strategically.

In its present form, our GNS exhibited a relative 2.5-fold increase in infiltration of the LCA, where there is dysfunctional GCX. This result is not consistent with our previous *in vitro* findings, where a 6–7 fold increase in GNS uptake was observed in rat fat pad endothelial cells after GCX dysfunction and a 4-fold increase in gold nanorods uptake was observed in human umbilical vein endothelial cells after GCX dysfunction.[5,6] One might assume that the less efficient uptake observed *in vivo* is attributed to opsonization by phagocytes like macrophages and other immune cells, or to clearance by the kidney and liver.[1,39] However, in the present study opsonization and clearance were avoided by coating the nanoparticles with PEG, which not only makes the particles biocompatible but also enhances their stealth capability.[1] In addition, the size

of the GNS falls within the 10–100 nm range at which primary clearance can be avoided.[1] Lastly, a 48-h time point for observation of GNS uptake after intravenous injection allows for sufficient time for the GNS to circulate and infiltrate vessel walls, before the GNS are clear by the animal body.[1]

To our knowledge, there is only one other published demonstration that nanoparticles can passively target pathologically remodeled vessel walls, written by Gomez-Garcia.[13] The Gomez-Garcia paper studied the manner in which nanoparticle localization to vessel walls depends on flow in situations of angiogenic conditions relevant to tumor vessels, which are inherently very leaky.[13] Due to the angiogenic context of the study, the Gomez-Garcia paper, like many other nanoparticle studies, utilizes nanoparticles that are large (200 nm) and, therefore, incompatible with GCX.[13] In contrast, our work shows passive nanoparticle targeting to vessel walls that are remodeled in a pro-atherosclerotic setting. As such, our work uniquely suggests synergistic importance of both flow conditions and the endothelial GCX in determining nanoparticle localization.

Confirmation of the causal relation between GCX expression and GNS infiltration should have been performed using GCX-deficient C57BL/6-background mice, for comparison to the normal C57BL/6-background mice. However, due to resource constraints, we utilized cultured endothelial cells. Human endothelial cells conditioned by a flow stimulus served as a relevant *in vitro* model.[10] One might be concerned that the *in vitro* studies are limited by the omission of several key components of targeted drug and nanoparticle delivery that natural exist *in vivo*. For example, *in vivo* there are many serum proteins that may bind to the GNS, increasing the effective GNS size or rendering minute differences in shape.[38] To mimic this and to overcome the limitation, the cell culture medium used in this study contained sufficient serum protein. One limitation that was not overcome in our cell culture experiment investigation of the role of GCX degradation in regulating trans-endothelial GNS infiltration, as was stated for the animal experiments, is the lack of exploration of the many components of the GCX. *In vivo* our focus was broadly on sialic acids and HS- and HA-associated *N*-acetylglucosamine. HS was the focus of the cell culture studies due to its abundance as a GCX component[26] and because we wanted to extend our previous work.[5–7] In low shear stress flow conditions (no flow: 0 dynes/cm^2), HS destabilization was not enough to promote GNS uptake by cultured human endothelial cells. This is likely because other components of the GCX are present[19] and blocking uptake. In high shear stress flow conditions (12 dynes/cm^2), enzyme-induced HS degradation significantly increased GNS uptake by the cultured cells. These results highlight the complexity of endothelial cell permeability to nanoparticles and the importance of paying attention to the GCX. Therefore, while other GCX components could have been considered in our *in vitro* GNS uptake experiments, the focus on HS lays an important foundation because attention to the endothelial GCX in drug and nanoparticle delivery is still not implemented in many studies. This work and other very recent reports[5–7,22,36] are providing growing evidence to show that GCX conditions play a key role in preventing or permitting endothelial cell and vascular targeting by drug carrying nanoparticles.

In summary, we successfully performed a partial LCA ligation to acutely disturb blood flow in a mouse vessel and we observed subsequent blood vessel remodeling and endothelial GCX dysfunction, both associated with atherosclerosis and cardiovascular disease, as well as passive targeting of GNS to affected areas. The GCX is often neglected in development of drug delivery approaches but this work shows that targeting dysfunctional vessels based on the GCX offers an innovative approach in cardiovascular disease therapy and prevention.

ELECTRONIC SUPPLEMENTARY MATERIAL

The online version of this article (https://doi.org/10.1007/s10439-020-02474-4) contains supplementary material, which is available to authorized users.

ACKNOWLEDGEMENTS

Solomon Mensah, Bijay Singh, Maeve X Enright, Paige Baldwin, Bailey L Ritchie, and James Lister of Northeastern University provided technical assistance and feedback. Northeastern University's Professor Thomas Webster, Professor Heather Clark, Assistant Professor Adam Ekenseair, the Department of Physics, and the Electronic Materials Research Institute shared equipment.

AUTHOR CONTRIBUTIONS

All authors contributed to data analysis, drafted and revised the article, and gave final approval of the version to be published. Specifically: M.J.C. and E.E.E. designed the experiments. M.J.C, R.M., C.C.O., A.A.N., I.C.H, and R.K. performed the experiments and analyzed the data. M.J.C. and E.E.E. interpreted the results of the experiments. M.J.C., R.M., N.N.B, and E.E.E drafted the figures and

manuscript. M.J.C., R.M., C.C.O., A.A.N., I.C.H, N.N.B, R.K., H.J., S.S., and E.E.E. edited, revised, and approved the final manuscript. H.J., S.S., and E.E.E. supervised the project. All authors agree to be accountable for all aspects of the work.

FUNDING

This work was funded by the National Institutes of Health (K01 HL125499 granted to EEE), the National Science Foundation (DGE-0965843 granted to SS and CMMI-1846962 granted to EEE), and the American Heart Association (18PRE33960461 granted to ICH). The funders had no role in data or information collection and analysis, decision to publish, or preparation of the manuscript.

CONFLICT OF INTEREST

Ming Cheng, Chinedu Okorafor, Alina Nersesyan, Ian Harding, Nandita Bal, Rajiv Kumar, Hanjoong Jo, Srinivas Sridhar, and Eno Ebong declare that they have no conflict of interest.

RESEARCH INVOLVING HUMAN AND ANIMAL RIGHTS

No human studies were carried out by the authors for this article. All institutional and national guidelines for the care and use of laboratory animals were followed and approved by the appropriate institutional committees.

REFERENCES

[1]Alexis, F., E. Pridgen, L. K. Molnar, and O. C. Farokhzad. Factors affecting the clearance and biodistribution of polymeric nanoparticles. *Mol. Pharm.* 5:505–515, 2008.

[2]Becker, B. F., M. Jacob, S. Leipert, A. H. Salmon, and D. Chappell. Degradation of the endothelial glycocalyx in clinical settings: searching for the sheddases. *Br. J. Clin. Pharmacol.* 80:389–402, 2015.

[3]Bennett, K. M., K. C. Kent, J. Schumacher, C. C. Greenberg, and J. E. Scarborough. Targeting the most important complications in vascular surgery. *J. Vasc. Surg.* 65:793–803, 2017.

[4]Bhadra, D., S. Bhadra, P. Jain, and N. K. Jain. Pegnology: a review of PEG-ylated systems. *Pharmazie* 57:5–29, 2002.

[5]Cheng, M. J., N. N. Bal, P. Prabakaran, R. Kumar, T. J. Webster, S. Sridhar, and E. E. Ebong. Ultrasmall gold nanorods: synthesis and glycocalyx-related permeability in human endothelial cells. *Int. J. Nanomed.* 319–333:2019, 2019.

[6]Cheng, M. J., R. Kumar, S. Sridhar, T. J. Webster, and E. E. Ebong. Endothelial glycocalyx conditions influence nanoparticle uptake for passive targeting. *Int. J. Nanomed.* 11:3305–3315, 2016.

[7]Cheng, M. J., P. Prabakaran, R. Kumar, S. Sridhar, and E. E. Ebong. Synthesis of functionalized 10-nm polymer-coated gold particles for endothelium targeting and drug delivery. *J. Vis. Exp.* 313:56760, 2018.

[8]DeBakey, M. E. Surgical treatment of atherosclerotic heart disease. *Am. J. Cardiol.* 63:9H–11H, 1989.

[9]Duwayri, Y., J. Goss, W. Knechtle, R. K. Veeraswamy, S. Arya, R. R. Rajani, L. P. Brewster, T. F. Dodson, and J. F. Sweeney. The readmission event after vascular surgery: causes and costs. *Ann. Vasc. Surg.* 36:7–12, 2016.

[10]Ebong, E. E., S. Kim, and N. DePaola. Flow regulates intercellular communication in HAEC by assembling functional Cx40 and Cx37 gap junctional channels. *Am. J. Physiol. Heart Circ. Physiol.* 290:H2015–2023, 2006.

[11]Ebong, E. E., F. P. Macaluso, D. C. Spray, and J. M. Tarbell. Imaging the endothelial glycocalyx in vitro by rapid freezing/freeze substitution transmission electron microscopy. *Arterioscler. Thromb. Vasc. Biol.* 31:1908–1915, 2011.

[12]Galyfos, G., K. Filis, F. Sigala, and G. Geropapas. Beta-blockers in vascular surgery patients: is the debate still going on? *J. Anesth.* 30:1031–1036, 2016.

[13]Gomez-Garcia, M. J., A. L. Doiron, R. R. M. Steele, H. I. Labouta, B. Vafadar, R. D. Shepherd, I. D. Gates, D. T. Cramb, S. J. Childs, and K. D. Rinker. Nanoparticle localization in blood vessels: dependence on fluid shear stress, flow disturbances, and flow-induced changes in endothelial physiology. *Nanoscale* 10:15249–15261, 2018.

[14]Harding, I. C., R. Mitra, S. A. Mensah, A. Nersesyan, N. N. Bal, and E. E. Ebong. Endothelial barrier reinforcement relies on flow-regulated glycocalyx, a potential therapeutic target. *Biorheology* 56:131–149, 2019.

[15]Kumar, S., D.-W. Kang, A. Rezvan, and H. Jo. Accelerated atherosclerosis development in C57Bl6 mice by overexpressing AAV-mediated PCSK9 and partial carotid ligation. *Lab. Invest.* 97:935, 2017.

[16]Kumase, F., Y. Morizane, S. Mohri, I. Takasu, A. Ohtsuka, and H. Ohtsuki. Glycocalyx degradation in retinal and choroidal capillary endothelium in rats with diabetes and hypertension. *Acta Med. Okayama* 64:277–283, 2010.

[17]Lewis, J. C., R. G. Taylor, N. D. Jones, R. W. St Clair, and J. F. Cornhill. Endothelial surface characteristics in pigeon coronary artery atherosclerosis. I. Cellular alterations during the initial stages of dietary cholesterol challenge. *Lab. Invest.* 46:123–138, 1982.

[18]Mathers, C. D., T. Boerma, and D. Ma Fat. Global and regional causes of death. *Br. Med. Bull.* 92:7–32, 2009.

[19]Mensah, S. A., I. C. Harding, M. Zhang, M. P. Jaeggli, V. P. Torchilin, M. J. Niedre, and E. E. Ebong. Metastatic cancer cell attachment to endothelium is promoted by endothelial glycocalyx sialic acid degradation. *AIChE J.* 65:e16634, 2019.

[20]Mitra, R., G. L. O'Neil, I. C. Harding, M. J. Cheng, S. A. Mensah, and E. E. Ebong. Glycocalyx in atherosclerosis-relevant endothelium function and as a therapeutic target. *Curr. Atheroscler. Rep.* 19:63, 2017.

[21]Mitra, R., J. Qiao, S. Madhavan, G. L. O'Neil, B. Ritchie, P. Kulkarni, S. Sridhar, A. L. van de Ven, E. M. C. Kemmerling, C. Ferris, J. A. Hamilton, and E. E. Ebong. The comparative effects of high fat diet or disturbed blood flow on glycocalyx integrity and vascular inflammation. *Trans. Med. Commun.* 2018. https://doi.org/10.1186/s41231-018-0029-9.

[22]Mockl, L., S. Hirn, A. A. Torrano, B. Uhl, C. Brauchle, and F. Krombach. The glycocalyx regulates the uptake of

nanoparticles by human endothelial cells in vitro. *Nanomedicine (Lond.)* 12:207–217, 2017.
[23]Nam, D., C.-W. Ni, A. Rezvan, J. Suo, K. Budzyn, A. Llanos, D. Harrison, D. Giddens, and H. Jo. Partial carotid ligation is a model of acutely induced disturbed flow, leading to rapid endothelial dysfunction and atherosclerosis. *Am. J. Physiol.* 297:H1535–H1543, 2009.
[24]Newman, C. B., D. Preiss, J. A. Tobert, T. A. Jacobson, R. L. Page II, L. B. Goldstein, C. Chin, L. R. Tannock, M. Miller, G. Raghuveer, P. B. Duell, E. A. Brinton, A. Pollak, L. T. Braun, F. K. Welty, *et al.* Statin safety and associated adverse events: a scientific statement from the American Heart Association. *Arterioscler. Thromb. Vasc. Biol.* 39:e38–e81, 2019.
[25]Nieuwdorp, M., M. C. Meuwese, H. Vink, J. B. Hoekstra, J. J. Kastelein, and E. S. Stroes. The endothelial glycocalyx: a potential barrier between health and vascular disease. *Curr. Opin. Lipidol.* 16:507–511, 2005.
[26]Oohira, A., T. N. Wight, and P. Bornstein. Sulfated proteoglycans synthesized by vascular endothelial cells in culture. *J. Biol. Chem.* 258:2014–2021, 1983.
[27]Potteaux, S., H. Ait-Oufella, and Z. Mallat. Mouse models of atherosclerosis. *Drug Discov. Today* 4:165–170, 2007.
[28]Pries, A. R., T. W. Secomb, and P. Gaehtgens. The endothelial surface layer. *Pflugers Arch.* 440:653–666, 2000.
[29]Prydz, K. Determinants of glycosaminoglycan (GAG) structure. *Biomolecules* 5:2003–2022, 2015.
[30]Rahbar, E., J. C. Cardenas, G. Baimukanova, B. Usadi, R. Bruhn, S. Pati, S. R. Ostrowski, P. I. Johansson, J. B. Holcomb, and C. E. Wade. Endothelial glycocalyx shedding and vascular permeability in severely injured trauma patients. *J. Trans. Med.* 13:117, 2015.
[31]Rehm, M., D. Bruegger, F. Christ, P. Conzen, M. Thiel, M. Jacob, D. Chappell, M. Stoeckelhuber, U. Welsch, B. Reichart, K. Peter, and B. F. Becker. Shedding of the endothelial glycocalyx in patients undergoing major vascular surgery with global and regional ischemia. *Circulation* 116:1896–1906, 2007.
[32]Reitsma, S., D. W. Slaaf, H. Vink, M. van Zandvoort, and M. G. A. oude Egbrink. The endothelial glycocalyx: composition, functions, and visualization. *Pflugers Arch.* 454:345–359, 2007.
[33]Singh, A., S. C. Satchell, C. R. Neal, E. A. McKenzie, J. E. Tooke, and P. W. Mathieson. Glomerular endothelial glycocalyx constitutes a barrier to protein permeability. *J. Am. Soc. Nephrol.* 18:2885–2893, 2007.
[34]Tarbell, J. M., and L. M. Cancel. The glycocalyx and its significance in human medicine. *J. Intern. Med.* 280:97–113, 2016.
[35]Tarbell, J. M., Z. D. Shi, J. Dunn, and H. Jo. Fluid mechanics, arterial disease, and gene expression. *Annu. Rev. Fluid Mech.* 46:591–614, 2014.
[36]Uhl, B., S. Hirn, R. Immler, K. Mildner, L. Mockl, M. Sperandio, C. Brauchle, C. A. Reichel, D. Zeuschner, and F. Krombach. The endothelial glycocalyx controls interactions of quantum dots with the endothelium and their translocation across the blood-tissue border. *ACS Nano* 11:1498–1508, 2017.
[37]Ushiyama, A., H. Kataoka, and T. Iijima. Glycocalyx and its involvement in clinical pathophysiologies. *J. Intensive Care* 4:59, 2016.
[38]Wang, H., Y. Lin, K. Nienhaus, and G. U. Nienhaus. The protein corona on nanoparticles as viewed from a nanoparticle-sizing perspective. *Wiley Interdiscip. Rev. Nanomed. Nanobiotechnol.* 10:e1500, 2018.
[39]You, J., J. Zhou, M. Zhou, Y. Liu, J. D. Robertson, D. Liang, C. Van Pelt, and C. Li. Pharmacokinetics, clearance, and biosafety of polyethylene glycol-coated hollow gold nanospheres. *Part Fibre Toxicol.* 11:26, 2014.